Three-Dimensional Solution Structure and Stability of Thioredoxin *m* from Spinach[†]

José L. Neira,[‡,§] Carlos González,[‡,||] Catherine Toiron,[||] Gonzalo de Prat-Gay,[⊥] and Manuel Rico*[,||]

Centro de Biología Molecular y Celular, Universidad Miguel Hernández, 03202 Elche (Alicante), Spain, Instituto de Investigaciones Bioquimicas, Fundacion Campomar and Facultad de Ciencias Exactas y Naturales, Universidad de Buenos Aires, Patricias Argentinas 435, 1405 Buenos Aires, Argentina, and Instituto de Estructura de la Materia, CSIC, 28006 Madrid, Spain

Received June 8, 2001; Revised Manuscript Received September 7, 2001

ABSTRACT: Proton NMR spectral resonances of thioredoxin *m* from spinach have been assigned, and its solution structure has been determined on the basis of 1156 nuclear Overhauser effect- (NOE-) derived distance constraints by using restrained molecular dynamics calculations. The average pairwise root-mean-square deviation (RMSD) for the 25 best NMR structures for the backbone was 1.0 ± 0.1, when the structurally well-defined residues were considered. The N- and C-terminal segments (1−13 and 118−119) and residues 41−49, comprising the active site, are highly disordered. At the time of concluding this work, a crystal structure of this protein was reported, in which thioredoxin *m* was found to crystallize as noncovalent dimers. Although the solution and crystal structures are very similar, no evidence was found about the existence of dimers in solution, thus confirming that dimerization is not needed for the regulatory activity of thioredoxin *m*. The spinach thioredoxin *m* does not unfold by heat in the range 25−85 °C, as revealed by thermal circular dichroic (CD) measurements. However, its unfolding free energy (9.1 ± 0.8 kcal mol^{-1}, at pH 5.3 and 25 °C) could be determined by extrapolating the free energy values obtained at different concentrations of guanidinium chloride (GdmCl). The folding−unfolding process is two-state as indicated by the coincidence of the CD denaturation curves obtained at far and near UV. The H/D exchange behavior of backbone amide protons was analyzed. The slowest-exchanging protons, requiring a global-unfolding mechanism in order to exchange, are those from β2, β3, and β4, the central strands of the β-sheet, which constitute the main element of the core of the protein. The free energies obtained from exchange measurements of protons belonging to the α-helices are lower than those derived from GdmCl denaturation studies, indicating that those protons exchange by local-unfolding mechanisms.

Thioredoxins belong to a family of proteins present in all living systems from eukaryotic to prokaryotic cells (*1*−*3*). A typical thioredoxin can be described as a small (∼10−12 kDa), monomeric, and heat-stable protein with an acidic isoelectric point, which functions as a disulfide oxidoreductase enzyme. Its catalytic mechanism involves a conserved pentapeptide sequence, -Trp-Cys-Gly-Pro-Cys-, and occurs via a reversible disulfide−dithiol reaction of the two SH groups (*2*). To date there are over 200 known sequences of different forms of thioredoxins with lengths ranging from 105 to 120 amino acids. Despite the large variation in primary structure among the members of the family, the location of these two cysteines in the active site is conserved. Furthermore, all members of the family with an available three-dimensional structure have a common fold (*1*, *4*), consisting of a central β-sheet flanked by α-helices. Thioredoxins are involved in a large number of important cellular processes (for a complete recent description of the biological activities of the thioredoxin family, see ref *5* and references therein) such as deoxyribonucleotide biosynthesis (*6*), regeneration of oxidative damage (*7*), activation of transcription factors (*8*), life cycle of *Escherichia coli* phages (*9*), and regulation of photosynthetic events (*10*).

Only one type of thioredoxin has been detected in bacteria or humans, but eukaryotic photosynthetic cells contains two, and possibly more, very distinct thioredoxins, some of them involved in the regulation of several chloroplastic enzymes (*11*, *12*). For instance, in spinach leaf chloroplasts, two types of thioredoxins have been identified: thioredoxin *f*, which activates the fructose-1,6-bisphosphatase (*13*), and thioredoxin *m*, which activates the NADP-dependent malate dehydrogenase (*11*). These two proteins are reduced by a ferredoxin-dependent thioredoxin reductase, light producing in turn the photoreduced ferredoxin (*14*). Also, in other photosynthetic cells there are cytosolic thioredoxins (named thioredoxin *h*), whose function remains unknown (*15*). Recently, the NMR[1] solution structure of thioredoxin *h* of green alga *Chlamydomonas reinhardtii* (*16*−*18*) has been reported; the structure is the typical thioredoxin fold. Within this general context, it is an interesting point to elucidate whether thioredoxin *m* of spinach leaves, a higher plant in the evolutionary scale, adopts also a similar fold to that of thioredoxin *h*.

In this study, we report on the ^{1}H assignment, the three-dimensional solution structure, and the stability of oxidized thioredoxin *m* (119 amino acids) from spinach leaves. Our findings show that the protein adopts the thioredoxin fold, with minor differences in the scaffolding of the β-sheet. The

[†] This work was supported by Project of Generalitat Valenciana GV-00-024-5 (to J.L.N.).

* Corresponding author: Instituto de Estructura de la Materia, Serrano 119, 28006 Madrid, Spain; phone 34 91 561 9400; fax 34 91 564 2431; e-mail rico@malika.iem.csic.es.

[‡] These two authors contributed equally to this work.

[§] Universidad Miguel Hernández.

[||] Instituto de Estructura de la Materia, CSIC.

[⊥] Universidad de Buenos Aires.

10.1021/bi011186x CCC: $20.00
Published on Web 11/17/2001

stability of the protein against heat and chemical denaturations has also been proven and shown to be remarkably large, as observed in other members of the family. These findings would set the basis for (a) studies to explain the high stability of thioredoxin *m* when compared to other members of the same family and (b) studies of the interaction between thioredoxin *m* and NADP-dependent malate dehydrogenase or fragments from it, directed to a better understanding of its role in basic plant photosynthetic processes. For these studies, the resonance assignment arrived at in this paper is absolutely crucial.

A crystal structure of thioredoxin *m* has been reported recently (*19*) that coincides practically with the one in solution determined here. Small structural and dynamic differences will be noted. Although thioredoxin *m* crystallizes as noncovalent dimers, we have not found any evidence for dimer formation in solution.

MATERIALS AND METHODS

Reagents and Protein Purification. Deuterium oxide (99 atom % in ^2H_2O) was obtained from Cambridge Isotope Laboratories, and TSP was from Sigma. Standard suppliers were used for all other chemicals. Water was deionized and purified on a Millipore system. Plasmid construction and protein purification was as described (*20*). Protein concentration was determined by UV spectrophotometry with the calculated extinction coefficients for model compounds (*21*).

NMR Spectroscopy. NMR samples were prepared by dissolving the lyophilized protein in a 9:1 $H_2O/^2H_2O$ solution. The solution was centrifuged briefly to remove insoluble protein and then transferred to a 5 mm NMR tube. Spectra were recorded on a Bruker AMX-600 spectrometer, working at a ^1H frequency of 600.13 MHz, at 35, 25, and 10 °C. The pH of the samples was adjusted by small amounts of ^2HCl and NaO^2H at a final value of 5.8, to compare with the solution structures of other thioredoxins. The pH was measured at the beginning and end of every experiment with a Russell glass electrode, without finding any difference between both measurements. Values of the pH reported here represent apparent values of pH, without correction for isotope effects. TSP was used as the internal chemical shift reference. Protein concentration was in the range 1−1.5 mM. Assignments are given in Table S1 of Supporting Information, at pH 5.8 and 25 °C.

One-dimensional spectra were acquired with 16K data points, averaged over 512 scans and with 7801.69 Hz spectral width (13 ppm). Two-dimensional spectra with a spectral width of 7801.69 Hz in both dimensions were acquired in the phase-sensitive mode by the time-proportional phase incrementation technique (TPPI) (*22*). Standard phase-cycling sequences were used to acquire the complete set of experiments in order to achieve assignments and structure elucidation. The double-quantum-filtered COSY experiment (*23*) was acquired with a data matrix size of 8K × 512 (t_2 and t_1, respectively) and 1 s of recycle delay, 128 scans per t_1 increment, and with the residual water signal attenuated by presaturation during the relaxation delay. TOCSY and NOESY experiments were acquired with a data matrix size of 4K × 512 (t_2 and t_1, respectively), with the MLEV17 spin-lock sequence (*24*) with 50 and 80 ms of mixing time in the TOCSY experiments. NOESY spectra (*25*) were collected with mixing times of 50 and 150 ms. Typically, 128 scans were acquired per t_1 increment in both types of experiments, with the residual water signal removed in both cases by the WATERGATE sequence (*26*). Data were zero-filled, resolution-enhanced, baseline-corrected with phase-shifted sine bell (DQF-COSY) or square sine-bell window functions (TOCSY and NOESY) optimized in each spectrum, and processed with the Bruker UXNMR software. ^1H NMR resonances were assigned by standard sequential assignment processes (*27*). The random coil chemical shift values of H_α protons were obtained from tabulated data in model peptides (*27*). $^3J_{HN\alpha}$ coupling constants of nonoverlapping signals were estimated by the analysis of TOCSY and NOESY spectra by the method of Wishart and co-workers (*28*). Qualitative exchange experiments were carried out by dissolving the lyophilized protein in ^2H_2O at pH 5.8 and 25 °C and acquiring a NOESY experiment with a mixing time of 150 ms during 20 h.

To check whether thioredoxin *m* forms dimers in solution, the 1.5 mM NMR sample was diluted 10-fold and the monodimensional spectra of the two solutions (1.5 and 0.15 mM) were compared. No change in either chemical shifts or line widths was observed (data not shown), which indicates that no aggregation takes place up to 1.5 mM concentration.

Amide Proton Exchange by NMR. Lyophilized samples of thioredoxin *m* were dissolved in 0.5 mL of ^2H_2O at pH 5.3, 25 °C, to detect the maximum number of amide protons. The exchange behavior was followed by the tandem method (*29*). Two-dimensional homonuclear COSY spectra in absolute mode (*30*) were acquired with increased delays for up to 5 days. During data acquisition the carrier frequency was set on the water signal, and the spectral width was 7801.69 Hz in both dimensions. The spectra were typically recorded with 2048 complex data points and 128 t_1 increments (128 scans per t_1 increment) by the TPPI method (*22*). The spectra were processed with the BRUKER−UXNMR software working on a SGI workstation. Prior to Fourier transformation, a mild square sine-bell window functions equal in all experiments was used. Polynomial baseline corrections were applied in both dimensions. The final 2D data matrix contained 2K × 1K data points. The volume integrals of the cross-peaks were calculated with the BRUKER software for each spectrum. Hydrogen exchange rates were determined by fitting the decay in cross-peak volumes vs time to the equation $I = A \exp(-k_{ex}t) + C$, where I represents the volume of the cross-peak, A is the amplitude of the exchange curve, k_{ex} is the observed exchange rate, t is the time expressed in minutes, and C is a constant, which takes into account the residual nondeuterated water and the threshold setting used in the intensity calculations. Data were fitted by the program Kaleidagraph (Abelbeck software) on a Macintosh computer. The full kinetics for the exchange reaction follows the Liderstrom−Lang scheme, according to

[1] Abbreviations: CD, circular dichroism; COSY, two-dimensional correlated spectroscopy; GdmCl, guanidinium chloride; NMR, nuclear magnetic resonance; NOE, nuclear Overhauser enhancement; NOESY, two-dimensional nuclear Overhauser enhancement spectroscopy; RMSD, root-mean-square deviation; TOCSY, two-dimensional total correlation spectroscopy; TPPI, time-proportional phase incrementation; TSP, [2,2,3,3-$^2H_4$]-3-(trimethylsilyl)propionic acid sodium salt.

$$\text{closed} \underset{k_{cl}}{\overset{k_{op}}{\rightleftharpoons}} \text{open} \xrightarrow{k_{int}} \text{exchanged}$$

where the closed form represents the exchange-incompetent form of the protein, and the open form is the exchange-competent form of the protein. In the final step of the above reaction, exchange takes place from the opening form according to the intrinsic constant, k_{int}. For each amide proton, this constant was calculated according to reported equations from model peptides (*31*). The other two constants, k_{op} and k_{cl}, are the rates of the opening and closing processes, respectively. Under our conditions (see legend to Table 3), exchange occurs by the so-called EX2 limit, in which $k_{ex} \gg k_{int}$, and k_{ex} is given by (*32*) $k_{ex} = (k_{op}/k_{cl})k_{int} = K_{op}k_{int}$, where K_{op} is the apparent equilibrium constant for the opening exchange-competent state. This K_{op} can be converted to apparent free energies by $\Delta G_{ex}^{app} = -RT \ln (K_{op}) = -RT \ln (k_{ex}/k_{int})$, where R is the gas constant and T is the temperature (in kelvins). It is important to note that this free energy is an apparent free energy, since its calculation relies upon the values of k_{int} of model peptides (*31*). We have assumed that all glutamic and aspartic residues are in the carboxylate form at this pH.

Determination of Three-Dimensional Structure. Analysis of the 50 and 150 ms NOESY spectra was carried out with the program XEASY (*33*). Cross-peaks were integrated by use of the integration routines of the XEASY package. Intensities were converted into upper distance bonds by use of the program CALIBA (*34*). Scaling factors were chosen to reproduce the correct distance limits for protons pairs separated by fixed distances, such as Hδ−Hϵ of aromatic rings or Hα−methyl in valine residues. Cross-peaks that could not be integrated due to either partial overlap or close proximity to the residual water signal were qualitatively assigned as strong, medium, and weak and were assigned distance constraints of 3.0, 4.0, and 5.0 Å, respectively. No constraints from hydrogen bonds or from coupling constants were used in the structure calculations. Initial structures were calculated from the NMR-derived upper bounds by the method implemented in the program DYANA (*35*, *36*). The best structures were used to solve for ambiguities in the cross-peak assignment. Thus, long-range and nonsequential NOE cross-peaks were assigned in several consecutive rounds of peak assignments and DYANA calculations. Stereoespecific assignments were obtained by comparison of the NOE patterns of experimental results with those expected from the structures obtained in the final stages of the distance geometry calculations. They are duly marked in the table of assignments (Table S1 of Supporting Information). For protons not stereoespecifically assigned and for methyl and aromatic protons, the usual pseudoatom corrections were applied. Finally, the best structures in the last round of DYANA calculations were further refined by restrained molecular dynamics with the program GROMOS (*37*) and the protocols of our laboratory for structure calculations (*38*−*40*), obtaining 25 structures. The atomic coordinates have been deposited in the Brookhaven Protein Data Bank, PDB code 1GL8. The program MOLMOL (*41*) was used in structure analysis, molecular graphic manipulations, and detection of possible hydrogen bonds. The criteria for hydrogen-bond formation were (a) proton−acceptor distance less than 2.0 Å and (b) donor−proton−acceptor angle less than 35°.

Circular Dichroic Experiments. Circular dichroic spectra were collected on a Jasco J720 spectropolarimeter fitted with a thermostated cell holder and interfaced with a Neslab RTE-110 water bath. The instrument was periodically calibrated with (+)-10-camphorsulfonic acid. Isothermal wavelength spectra were acquired at a scan speed of 50 nm/min with a response time of 1 s and averaged over six scans at 25 (± 0.1) °C. The corresponding amount of protein was dissolved in 20 mM phosphate at pH 5.3. The reported pHs in these experiments were the readings from the pH-meter. Far-UV measurements were performed with 20−30 μM protein in a 0.1 or 0.2 cm path length cell. Near-UV spectra were acquired with 30−40 μM protein in a 0.2 or 0.5 cm path length cuvette, which were corrected by subtracting the proper baseline in all cases. Concentration dependence experiments were carried out in the range 10−150 μM. No differences in the CD signals were observed in that range (data not shown). Ellipticities are expressed in units of degrees centimeters^2 per decimole, according to the expression $[\Theta] = \Theta/10lcN$, where Θ is the observed ellipticity, c is the molar concentration of the protein, l is the cell path length (in centimeters), and N is the number of amino acid residues in the sequence.

Thermal denaturation experiments were performed at a heating rate of 50 °C/h and a response time of 8 s. Thermal scans were collected in the far-UV region at 222 nm from 25 to 85.0 °C in 0.2 cm cells with a total protein concentration of 20−30 μM at pH 5.3. The solution conditions were the same as those reported in the far-UV experiments. The reversibility of thermal transitions was checked by recording a new scan after cooling of the thermally denatured sample and comparing the new scan with the spectrum obtained before heating. The possibility of drifting of the CD spectropolarimeter was checked by running two samples containing buffer before and after the thermal experiments. No difference was observed between the scans.

GdmCl titrations were carried out under the same conditions as the exchange experiments, that is, pH 5.3 and 25 °C, by dissolving the proper amount of the denaturant from an 8 M stock solution and leaving the solution overnight to equilibrate. Spectra were acquired at a scan speed of 50 nm/min, and six scans were recorded at 25 °C. The response time was 2 s. The path length of the cell was 0.1 cm, with a protein concentration of 20−30 μM. For the experiments in the near-UV, 0.2 cm path length cuvettes were used. Spectra were corrected by subtracting the baseline in all cases. The chemical denaturation sample is fully reversible, as demonstrated by the sigmoidal curves obtained by starting from diluted 6 M GdmCl (data not shown).

Analysis of Denaturation Curves and Free Energy Determination. Denaturation curves were analyzed with a two-state model for the native/unfolded equilibrium, according to the linear extrapolation model $\Delta G = m([U]_{50\%} - [U])$, where ΔG is the free energy of denaturation, [U] is the denaturant concentration, and $[U]_{50\%}$ is the concentration at the midpoint of the transition. The denaturation data obtained by CD (far and near) were fitted to the two-state equation (*42*)

$$\Theta = \frac{(\Theta_N + \Theta_D e^{-\Delta G/RT})}{(1 + e^{-\Delta G/RT})}$$

where Θ_N and Θ_D are the corresponding ellipticities of the folded (N) and unfolded states (U), respectively, for which a linear relationship with denaturant (i.e., $\Theta_N = \alpha_N + \beta_N$[U] and $\Theta_D = \alpha_D + \beta_D$[U]) is admitted; *R* is the gas constant and *T* is the temperature in kelvins. Fitting by nonlinear least-squares analysis was carried out by using the general curve-fit option of Kaleidagraph (Abelbeck software) on a Macintosh computer. The results are indicated in Table 4.

RESULTS

^{1}H NMR Sequential Assignments. Thioredoxin (13 kDa) is just around the high molecular weight limit for NMR structure determination, with only unlabeled samples. Nevertheless, due to the high content of secondary structure elements, the overlapping of resonance lines is not too severe, so that the assignment could be carried out by the strategy based upon homonuclear experiments (*27*).

A summary of the observed interresidue sequential NOE connectivities for oxidized thioredoxin *m* is shown in Figure 1. Continuous sequential backbone−backbone NOEs facilitated the assignment for the majority of the backbone resonances, except for those regions where they were absent. Especially difficult was the region involving residues 80−87, belonging to a helical structure (see below), where the Hα resonances of several residues were close to the water signal (see Table S1 of Supporting Information) or obscured by overlapping with other resonances. Similar difficulties were found for the pair Ser118-Pro119. The highly flexible segment comprising the first 13 N-terminal residues could not be assigned unambiguously because of the severe overlapping in the region where those amide protons appear. Resonances in that region were tentatively assigned on the basis of similarity of the observed chemical shifts with those of random-coil models (*27*). All evidence (shifts and line widths) points toward that region being totally unstructured.

Residues belonging to the *β*-strands could be easily assigned because of the strong sequential αN (*i*, *i* + 1) NOEs and interstrand long-range NOEs. Figure 2 shows the *β*-strand connectivities within the *β*-sheet. Some NOE connectivities, which were to be expected on the basis of scaffolding of the *β*-sheet, could not be observed because of their proximity to either the diagonal or the residual water signal, such as that between the Hα protons of Trp38 and Pro86.

Amino acid residues in the first helix (residues 22−29) were difficult to assign because of overlapping of NH and Hα chemical shifts of adjacent residues. For instance, residues Trp22 and Lys23 have very similar Hα chemical shifts, as it happens also with those of Glu24 and Phe25 (Table S1 of Supporting Information). Similar difficulties were found in the fourth helix: the NH resonances of residues Thr108 and Leu109 are identical (7.39 ppm), and also those of Lys106 and Thr110 (8.88 ppm). Conversely, residues in the second helix following the ones belonging to the active site were easily followed through the sequential NH−NH NOE connectivities.

We also experienced some difficulty in assigning the active-site region. Sequential assignments of residues up to Trp 41 were straightforward. The NH of Cys42 could be identified from a weak, but distinctive, NN (*i*, *i* + 1) NOE connectivity between Trp41 and Cys42. We could not assign the resonances of Hα protons of Gly43 and Pro44 until we had almost finished the assignment of the protein. However, the NH chemical shift of Gly43 could not be identified. Similar results have been observed in the oxidized forms of *E. coli* thioredoxin (*43*) and the thioredoxin *h* form *C. reinhardtii* (*16*). The sequential connectivities between Pro44 and Cys45 are obscured due to overlapping with other resonances.

Among the eight proline residues of thioredoxin *m*, only Pro86 was found to be in a cis configuration, as evidenced from the intense NOE contact between the Hα proton of Ile85 and the Hα proton of Pro86 (Figure 1). There is no evidence of minor populations in the trans conformation. The remaining prolines showed intense NOEs between their Hδ protons and the Hα of the preceding residue, as expected for a trans conformation.

Secondary Structure Pattern Recognition and Protein Main-Chain Fold. Figure 1 provides additional qualitative information useful in the identification of secondary structure along the protein chain. This information is the following: (a) an estimation of the $^3J_{HN\alpha}$ of nonoverlapping signals obtained by applying the procedure developed by Wishart and co-workers (*28*) to TOCSY and NOESY experiments; (b) amide proton exchange rates observed for a period of 20 h to identify hydrogen-bonded protons; and finally, (c) conformational shifts [Hα chemical shifts minus random coil values (*27*)]. By using these data and the complete set of long-distance NOEs, we were able to characterize the elements of secondary structure of thioredoxin *m*, which consists of four helices and five *β*-strands.

The four helices roughly spanning residues 22−28 (α1), 50−60 (α2), 72−82 (α3), and 106−117 (α4) can be inferred from Figure 1 by (i) strong or medium NN (*i*, *i* + 1), medium αN (*i*, *i* + 2), and medium α*β* (*i*, *i* + 3) connectivities; (ii) coupling constants < 6 Hz; (iii) negative conformational shifts; and (iv) amide protons protected against exchange after 20 h.

The presence of five *β*-strands spanning residues 13−17 (*β*1), 32−38 (*β*2), 63−69 (*β*3), 86−92 (*β*4), and 96−102 (*β*5) could be inferred from (i) long-distance NOEs involving backbone amides and Hα protons of residues located in different *β*-strands (Figure 2) [*β*3 tightly associates with *β*2 in a parallel manner, as well as *β*3 with *β*1 (see below), and *β*4 is associated with *β*5 and *β*2 in an antiparallel fashion]; (ii) coupling constants > 6 Hz (Figure 1); (iii) positive conformational shifts; and (iv) consistency between the observed slow-exchanging protons after 20 h and the hydrogen-bond scaffolding characteristic of the *β*-sheet conformation (Figure 2).

Residues 13−17 have large positive conformational shifts (Figure 1), but no evidence of long-range contacts of this region with the other *β*-strands was found (Figure 2), nor were slow-exchanging protons detected in the strand (Figure 1). Long-range contacts were observed, however, between the side chain of Val14 and Tyr66, indicating the proximity between both residues. Similar behavior was observed in the thioredoxin *h* of *C. reinhardtii* (*16*), although long-range main-chain−main-chain NOEs were also detected in that case.

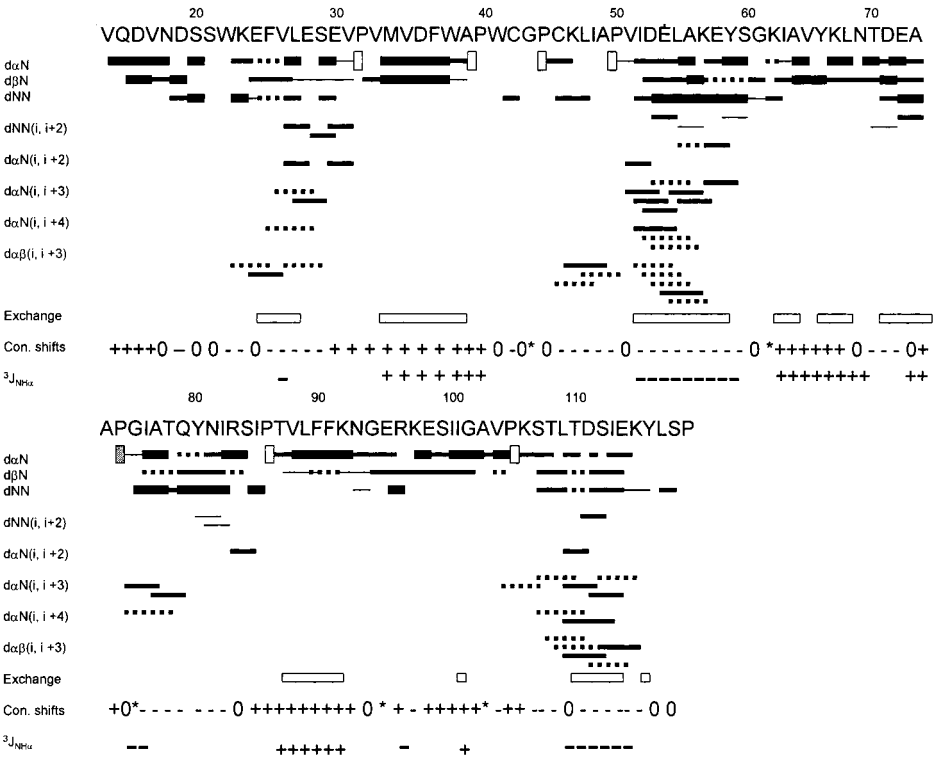

FIGURE 1: Summary of NMR data. NOEs are classified into strong, medium, or weak, according to the height of the bar underneath the sequence. The corresponding sequential Hα NOE with the following Hδ of the proline residue are indicated by an open bar in the row corresponding to the αN (*i*, *I* + 1) NOEs. The white squares indicate those residues that were detected after 20 h of exchange; exchange was initiated by dissolving the protein in ^2H_2O at pH 5.8 and 35 °C. Residues whose conformational shifts (see text) are larger, positive or negative, are represented by a + or −, respectively; 0 indicates those residues whose conformational shifts are lower (positive or negative) than 0.1; and asterisks indicate the glycine residues, with two different chemical shifts for each Hα proton. Amide proton−α-proton vicinal spin−spin coupling constant, $^3J_{NHH\alpha}$, are represented by a + for those residues with a value larger than 6 Hz and − for those with a value lower than 6 Hz.

Solution Structure Calculations of Thioredoxin m of Spinach. Structure calculation followed the protocol described under Materials and Methods. Several repeated rounds of long-range and nonsequential NOEs were assigned and converted to distance constraints to use as input data in DYANA. Distance constraints were derived from the 50 ms NOESY experiment. The best DYANA structures together with the NOESY spectra were used to assign stereoespecifically the methyl protons of six out of 11 valine residues, and the $\beta\beta'$ protons of appropriate residues showing different chemical shift and nonoverlapping signals. The resulting structures were subjected to another DYANA calculation and further refined by restrained molecular dynamics with GROMOS to generate 25 energy-minimized NMR solution structures. Table 1 summarizes the number of structurally relevant intraresidual, sequential, and medium- and long-range constraints. In Table 2, the residual violations and the potential energies of the calculated structures are given. The average pairwise RMSD values for all backbone atoms and heavy atoms between residues 13 and 117 were 1.4 ± 0.3 and 2.1 ± 0.4 Å, respectively. The region between residues 41 and 49 is poorly defined. When these residues are excluded, the global RMSD is 1.1 ± 0.1 Å for the backbone and 1.8 ± 0.2 Å for the heavy atoms. Figure 3 (top) shows the backbone conformations in the final 25 energy-minimized structures superimposed for minimal RMSD over the structurally well-defined residues 13−117 with the first 13 and last residues omitted for the sake of clarity. Figure 4 describes the backbone (ϕ, ψ) dihedral angles of each residue in the 25 energy-minimized structures.

Analysis of the Three-Dimensional NMR Solution Structure of Thioredoxin m. The structure of thioredoxin *m* is formed by a five-stranded β-sheet surrounded by four helices, with the first 13 residues disordered. The five strands in the β-sheet are arranged in a parallel and antiparallel manner (Figure 2). Well-defined secondary structure elements account for 80% of its structure. Except for the first 13 residues and the loop region following α3, all residues are involved in either β-strands, helices, or turns. The extension of the different elements of secondary structure as determined by the structure calculation matches very closely the one derived qualitatively in the previous section, by use of the chemical shift, NOE, and exchange data information.

(*i*) α-*Helices.* The four α-helices are displayed on the external surface of the globular molecule. All helices are rather regular with only minor deviations for the main-chain torsion angles, ϕ and ψ, in relation to the standard α-helical values. The length of the helices is very similar in the NMR structures and in the crystallographic one, with the exception of the α2 helix (*19*). In the crystal structure this helix extends from residues 44 to 60, while in solution the helix runs only from 49 to 60.

(*ii*) β-*Sheet.* The five-stranded pleated β-sheet forms the core of the molecule, with most residues being highly hydrophobic. The sheet is twisted and composed of parallel (p) and antiparallel (a) strands with the arrangement β1p β3p β2p β4a β5a. In Figure 2, the observed NOE connectivities are represented.

Residues 13−17 could not be defined at first as a part of the β-sheet, due to the absence of backbone−backbone NOE

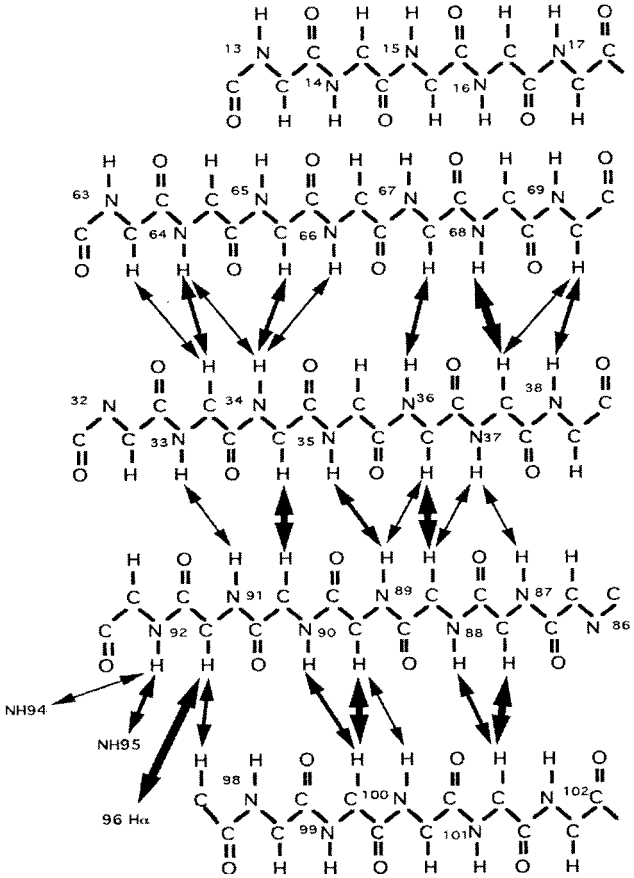

FIGURE 2: Alignment of the five β-sheets of thioredoxin *m*. Long-distance NOEs observed in NOESY spectra are shown by continuous double arrows.

Table 1: NMR Structure Constraints Summary

type of constraints[a]	no. of constraints: total	<3.5 Å	3.5−4.5 Å	>4.5 Å[b]
intraresidual ($\|i-j\|=0$)	174	22	92	60
sequential ($\|i-j\|=1$)	336	87	80	169
medium-range ($2<\|i-j\|<5$)	265	8	49	208
long-range ($\|i-j\|>5$)	381	6	18	357
all	1156			

[a] *i* and *j* represent two residues in the primary sequence. [b] The upper limit is 5.0 plus appropriate pseudoatom corrections (see text).

Table 2: Residual Constraints Violations in the Final 25 Structures

range (Å)	avg no. of distance constraint violations
0.00−0.25	132.2
0.25−0.50	43.7
0.50−0.75	4.4
0.75−1.00	0.7
>1.00	0.0
maximum violation (Å)	0.7
avg sum of violations (Å)	32.7

	avg	range
total energy (kJ mol^{-1})	−3432	−3820 to −3130
Lennard-Jones energy (kJ mol^{-1})	−1540	−1781 to −1110
NOE term (kJ mol^{-1})	330	286 to 372

contacts with the region 63−69 and to the lack of protection. However, the presence of side-chain−side-chain contacts between some residues of β3 and those of the region 13−17, as well as the downfield shift observed for most of the latter protons (Table S1 of Supporting Information) are in favor of defining that segment as a β-strand (β1). The absence of observed NOE connectivities could be due to signal overlapping, proximity to residual water signal, or a looser secondary structure, as shown in a thioredoxin of *C. reinhardtii* (*16*). The remaining four strands present a regular and well-defined conformation, almost identical to the X-ray structure (Figure 3, bottom).

(*iii*) *Packing of Secondary Structure Elements and β-Turns.* There are four β-turns in thioredoxin *m* and a reverse turn, which involves cis Pro86. Most of these turns are rather flexible, but in general, the most populated conformer in the NMR ensemble coincides with the X-ray conformation.

Helices α1 and α3 pack on one side of the β-sheet and α2 and α4 on the opposite side. The side chains form hydrophobic clusters on either side of the β-sheet. A first cluster involves the side chains of Trp22 (α1), Val26 (α1), Val35 (β2), Phe37 (β2), Ile76 (α3), Tyr80 (α3), Ile82 (loop), Phe91 (β-hairpin), and Arg96 (β-hairpin). The aromatic side chains of this cluster are arranged in a tetrahedral geometry and are the most important contributors to the cluster stability. Similar arrangements occur in the corresponding residues of the *E. coli* thioredoxin (*43*,*44*) and in thioredoxin *h* of *C. reinhardtii* (*17*,*18*). On the opposite side of the β-sheet, the cluster is formed by Ile52 (α2), Val65 (β3), Val88 (β4), and Tyr59 (at the C-cap of α2). This cluster is organized around the aromatic chain of Tyr59, which is at the end of a groove formed by helices α2 and α4.

Helices α2 and α4 pack against each other via hydrophobic interactions and through a network of ionic interactions involving Glu54, Glu58, and Lys106. On the basis of the large number of salt bridges present in α4 and in computer simulations (*45*), it has been suggested that α4 could act as a protective element for the whole molecule (*46*). Those interactions would prevent the fraying of the C-terminus of helix α4 and then the denaturation of the whole protein. Helices α1 and α3 do not interact as extensively as α2 and α4, although NOE connectivities do exist between the side chains of Trp22 and Tyr80 and between Ala73 and Asn18.

(*iv*) *Redox-Active Site.* The active site involves residues Trp41-Cys42-Gly43-Pro44-Cys45, at the N-terminus of α2. It is a flexible region, as judged by a local backbone-atom RMSD of 1.5 ± 0.3 Å. Only the (ϕ, ψ) dihedral angles of Trp41 are well-defined, the others being completely disordered (Figure 4). The active-site side chains protrude from the surface of the protein and display very few interactions with the rest of the structure. The only interaction present in the calculated structures was the one between the indole proton of Trp41 and the side chain of Asp71. However, no NOE connectivities could be observed between the two residues. Conversely, the preceding and the following part of the segment containing the residues at the active site are held tight through long-range interactions. The preceding region is β2, which is a constituent of the core of the protein, and the following region is α2, which makes strong interactions with α4 and the rest of the β-strands.

Comparison with the X-ray Structure. The main difference between the crystal and solution structure of thioredoxin *m* is that in the first case a noncovalent dimer is formed (*19*), while no evidence has been found in the latter to support dimerization. The RMSD between the average solution structure and each subunit of the X-ray structure is 1.3 Å

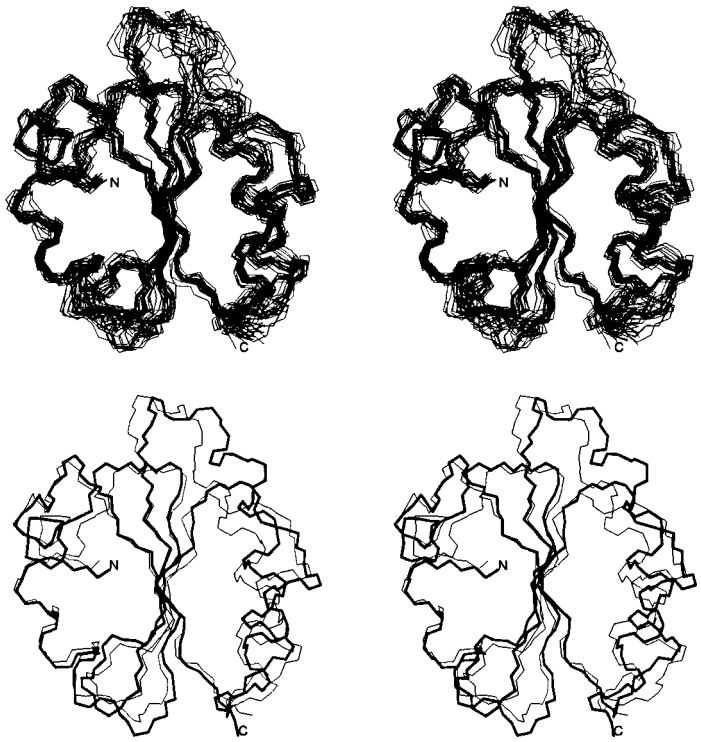

FIGURE 3: Stereoview of the polypeptide backbone of thioredoxin *m*. (Top) Final 25 energy-minimized NMR structures superimposed over residues 13−117. (Bottom) Superpositions of the average NMR structure and the crystallographic one (*19*).

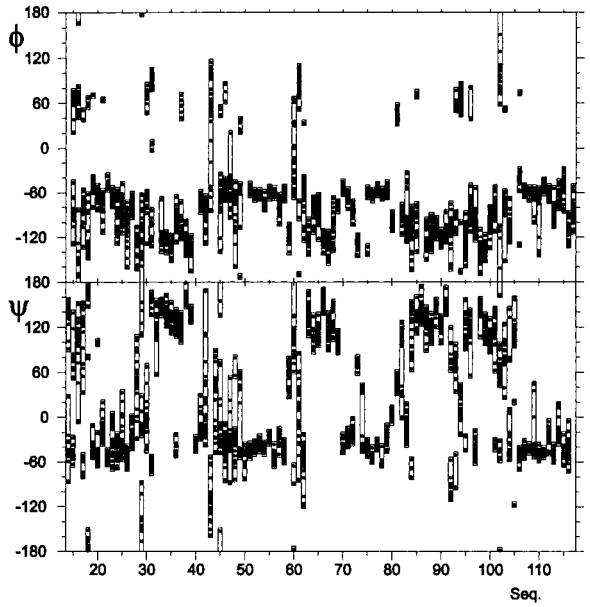

FIGURE 4: Backbone (ϕ, ψ) angles for each residue in the 25 best NMR structures. Each dot indicates the value in one NMR structure, and the bar indicates the range of NMR values.

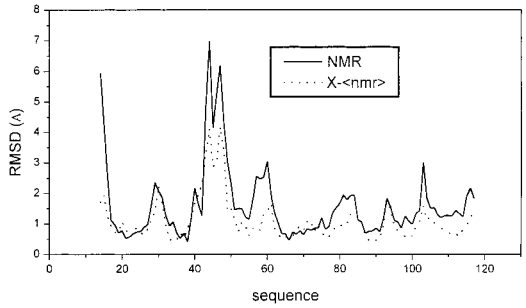

FIGURE 5: RMSD per residue between the 25 NMR structures (solid line) and between the X-ray and the average solution structure (dashed line).

for the well-defined region, only slightly larger than the RMSD between the different structures in the NMR ensemble. The largest differences between the structures are located in regions where the solution structure is poorly defined (Figure 5). From that we may conclude that there are not large conformational changes upon dimer formation in the crystal.

Dimerization in human thioredoxin was interpreted as a possible regulatory mechanism (*47, 6*), a hypothesis that was challenged by NMR-based studies (*48*). To check whether thioredoxin *m* from spinach forms dimers in solution, we have used four different approaches covering a complete range of protein concentration. First, we have carried out concentration-dependence CD experiments in the range 10−150 μM; no differences in the shape or the intensity (after normalization) of the CD signals were observed in that concentration range (data not shown). Second, the 1.5 mM NMR sample was diluted 10-fold and the monodimensional spectra of the two solutions (1.5 and 0.15 mM) were compared. No change in either chemical shifts or line widths was observed; for example, the line widths for the methyl groups of Val26 and the methyl γ group of Ile76 (the most upfield-shifted protons in thioredoxin *m*; see Table S1 in Supporting Information) at both concentrations are 25 Hz, in the range observed for the same resonances in other monomeric thioredoxins, where a value of 20 Hz is found (*49*). Lower concentrations than 0.15 mM yielded poor signal-to-noise NMR spectra. Thus, both sets of experiments (CD and NMR) indicate that no aggregation is taking place from 10 μM up to 1.5 mM concentration. Third, a calculation was performed in order to list the possible intermolecular NOEs in a dimer like the one in the crystal structure, and a

Table 3: Amide Proton Exchange[a]

NH residue	secondary structure	k_{int}[a] (min^{-1})	k_{ex}[b] (min^{-1})	ΔG_{ex}^{app}[c] (kcal mol^{-1})
Glu24	α1	7.93	0.0015 ± 0.0004	5.0 ± 0.4
Val33[d]	β2		slow	>6.0
Asp36[d]	β2		slow	>6.0
Ser60	α2	8.49	0.0069 ± 0.0004	4.2 ± 0.3
Lys67	β3		slow	>6.0
Ala73	α3	2.28	0.00047 ± 0.00007	5.0 ± 0.5
Tyr80	α3	2.75	0.0014 ± 0.0005	4.5 ± 0.4
Thr87	β4	10.94	0.0003 ± 0.0001	6.0 ± 0.6
Leu89	β4		slow	>6.0
Phe91	β4		slow	>6.0
Lys92	β4		slow	>6.0
Ile100	β5	1.28	0.0022 ± 0.0004	3.8 ± 0.3
Ser112	α4	5.00	0.0025 ± 0.008	4.5 ± 0.4
Val116	α4	2.28	0.0011 ± 0.0007	4.3 ± 0.5

[a] Calculated according to Englander and co-workers at pH 5.3 and 298 K (*31*). [b] Errors are fitting errors to the exponential decay. [c] Free energies are calculated assuming EX2 mechanism in thioredoxin *m*. The mechanism of exchange is EX2, as can be concluded from several observations (*61*). First, in an EX1 mechanism, all the observed exchange rates must be similar (*62*), while in our conditions the exchange rates are very different. Second, the apparent free energies determined for Ala73 and Thr87 are identical, within error, despite the large differences in the values of k_{int}. [d] These signals overlap in the COSY experiments.

search for those NOEs was conducted for tracing them in the spectra, which was unsuccessful. In fact, the number of NOEs left unassigned was very low indeed. Finally, gel-filtration experiments carried out during purification of thioredoxin *m*, on a gel-filtration Superdex G75 (26/60) column (Amersham Pharmacia Biotech), showed that thioredoxin *m* elutes at the volume expected for a protein with a molecular weight of 12−13 kDa in the range of concentrations explored, 50−200 μM. These facts further confirm the absence in solution of a dimerization of thioredoxin *m* like the one observed in the crystal.

Amide Proton Exchange in Thioredoxin m. The exchange rate of residues Lys67 (β3), Leu89 (β4), Phe91 (β4), Lys92 (β-bulge), and Val33 and Asp36 (β3) could not be determined because their exchange rates were too slow to be measured under our conditions (i.e., the intensity of their respective cross-peaks decreased less than 10% during the time of the experiment) (Table 3). These residues are deeply buried in the core of the protein and their exchange takes place by a global-unfolding mechanism. There were other residues whose exchange rates could not be measured due to poor magnetization transfer through the *J* coupling in the absolute-mode COSY experiment. The exchange rates and unfolding free energies of the remaining residues are collected in Table 3. We have probes at every element of secondary structure but β1. For α1, monitored by Glu24, the free energy is 5.0 kcal mol^{-1}. For α2, it is 4.2 kcal mol^{-1}, as monitored by Ser60, the only residue for which exchange could be measured. In α3, residues Ala73 and Tyr80 could be observed displaying very close free energies, probably indicating that both residues exchange by the same local-unfolding event. Finally, Ser112 and Tyr116 map the stability of α4 in the middle of the helix and at its C terminus, with very similar free energies. Ile100 (β5) was the only residue involved in the β-sheet whose exchange rate could be measured, probably due to the fact that the β5 is not involved in the central scaffolding of the β-sheet.

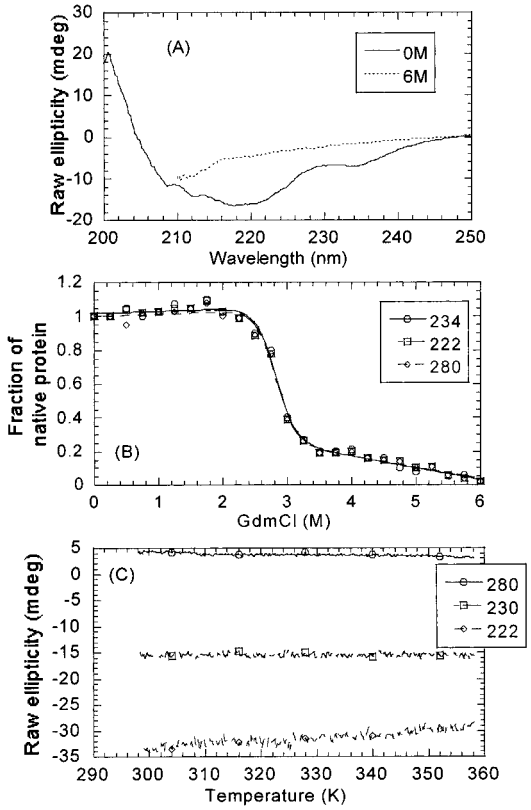

FIGURE 6: (A) Far-UV CD at 0 and 6 M GdmCl at 25 °C. (B) GdmCl denaturation followed by far- and near-UV (pH 5.3, 25 °C). (C) Thermal denaturation of thioredoxin *m* at different wavelengths (the units are arbitrary).

Table 4: Thermodynamical Parameters for GdmCl Denaturation[a]

spectroscopic probe	*m* (kcal mol^{-1} M^{-1})	$[GdmCl]_{50\%}$ (M)	ΔG_{water} (kcal mol^{-1})
far-UV CD (234 nm)	3.4 ± 0.5	2.88 ± 0.03	9.8 ± 0.9
far-UV CD (222 nm)	3.1 ± 0.3	2.83 ± 0.03	8.8 ± 0.8
near-UV CD (280 nm)	3.2 ± 0.4	2.87 ± 0.04	9.2 ± 0.8
mean	3.2 ± 0.4	2.86 ± 0.03	9.1 ± 0.8

[a] Errors are fitting errors to the two-state equation (see Materials and Methods section).

CD Measurements of Thioredoxin m Folding and Stability. The folding and stability of thioredoxin *m* under the same exchange NMR conditions were examined by near- and far-UV CD and thermal denaturation. In the absence of denaturant, native thioredoxin *m* has a very intense far-UV CD spectrum with a minimum at 220 nm and a smaller one at 234 nm (Figure 6A). The latter must be due to the presence of tryptophan residues in the sequence, as it has been reported for other proteins (*50, 51*). When the denaturant concentration was increased, the ellipticity decreased, showing sigmoidal behavior. The thermodynamic parameters obtained from the fitting to the two-state equation at several wavelengths are given in Table 4 (Figure 6B).

The near-UV spectrum of native thioredoxin is very intense, as could be expected for a protein with six tyrosine residues, three tryptophans, and five phenylalanines (data not shown). There is a clear maximum at 280 nm. No near-UV signals could be observed, however, at 6 M GdmCl. The chemical denaturation followed by near-UV also showed sigmoidal behavior (Figure 6B).

Table 5: RMSD between Thioredoxin *m* from Spinach Leaves and Other Thioredoxins[a]

atoms	*E. coli*	*Anabaena*	*B. acido-caldarius*	*C. rein-hardtii*	human
backbone atoms[b]	1.5	1.3	1.9	1.8	1.7
β-sheet[c]	0.6	0.7	1.1	0.9	1.4
α helices[d]	1.4	1.1	1.7	1.5	1.7

[a] The PDB data entries are as follows: for *E. coli* (molecule A), 2TRX (*44*); thioredoxin 2 from *Anabaena* (*54*), 1THX; thioredoxin from *B. acidocaldarius* (*46*), 1QUW; thioredoxin *h* from *C. reinhardtii* (*19*), 1TOF; and human thioredoxin (*55*), 1TRS. The protein sequences were aligned by a least-squares fit of the backbone atoms. Sequence numbers in parentheses refer to thioredoxin *m* from spinach leaves. [b] Residues 13−41 and 49−117 (residues between 41 and 49 are poorly defined). [c] Residues 13−17 (β1), 32−38 (β2), 63−69 (β3), 86−92 (β4), and 96−102 (β5). [d] Residues 22−30 (α1), 41−60 (α2), 72−84 (α3), and 107−117 (α4).

Up to the highest temperature examined, no sigmoidal temperature dependence of the ellipticities was observed. The signal at 222 nm just decreased slightly in a linear and monotonic way with increasing temperature in the examined range (Figure 6C).

DISCUSSION

Comparison of the Thioredoxin m Structure with Those of Other Thioredoxins. A qualitative inspection of the structure of this thioredoxin of plant origin with those previously described belonging to inferior organisms indicates that the overall fold is very similar indeed (Table 5). The structural similarity observed in the main chain is not surprising because of the high structural homology found within the thioredoxin family (*1*) and the high sequence similarity between thioredoxin *m* from spinach leaves and thioredoxin *h* of *C. reinhardtii* (50%), whose fold fits well within the overall thioredoxin fold (*16*). In general, the superposition of each known thioredoxin with the one from spinach reveals that the fit is best for α-helices and that there are minor differences in the β-sheet, due to the looser structure in β1 of thioredoxin *m*.

Among the highly conserved residues, the hydrogen-bond pattern and side-chain conformations are also maintained. There are some conspicuous structural features of other thioredoxins that are also present here, e.g., the unusual left-handed helical conformation adopted by Glu30 and the central role played by Tyr59 in organizing in its surroundings a cluster of hydrophobic residues in which residues from helices 2 and 4 are involved. Similar reasoning can be made on the other hydrophobic cluster (see before) located in a different region of the protein: the residues change from one thioredoxin to the other, but the orientation of the side chains is rather the same. There are, however, some small differences, apart from that already mentioned about the flexible strand β1, like those in the region of α3, which appears in our case more distorted than in *E. coli* thioredoxin, where this region comprises two turns of α-helix and two turns of a 3_{10} helix (*43, 44*), and in thioredoxin from *C. reinhardtii*, where a quite regular α-helix with the expected CO_i-NH_{i+4} hydrogen-bond scaffolding is observed (*17, 18*).

The similarity between the structure of spinach thioredoxin *m* and those of other known thioredoxins extends also to the active site, where most residues are conserved. In the analyzed thioredoxins, the active site is surrounded by highly hydrophobic residues that are thought to be important in the binding to other proteins (*52, 53*). In thioredoxin *m* these residues are Trp38, Ile85, Pro86, and those in the segment Ile100−Ala103. Although those residues are not conserved among the members of the family, the orientations of the particular side chains are essentially the same. It should be interesting to elucidate in future studies whether these residues are important for the binding of thioredoxin *m* to NADP-dependent malate dehydrogenase or even to fructose-1,6-bisphosphatase.

In the active site, the backbone of both catalytic cysteine residues is different. Cys45 has a well-defined conformation, and that of Cys42 is very flexible. A similar fact has been observed in all other thioredoxin solution structures (*19, 44, 48*), which must be an intrinsic characteristic of their active site. The side-chain torsional angle χ1 for Cys 42 is also spread among several conformations with a mean value of 150°. This value is similar to that found for this cysteine residue in *E. coli* (*44*) and *B. acidocaldarius* (*46*) thioredoxins, but it differs from the one found in thioredoxin from *C. reinhardtii* (*17,18*). The reason for this discrepancy might be related to the different reactivity of the members of thioredoxin family shown during the first step of the enzymatic reduction, when Cys42 is involved. Conversely, Cys45 has a similar χ1 value among all thioredoxins known so far, namely, −52°. The S−S disulfide bridge has a unique right-handed conformation, which is similar to the one observed in other oxidized thioredoxins (*45, 46, 54, 55*).

Dynamical Aspects. We have found that amide protons with exchange rates susceptible to being measured are all hydrogen-bonded (Table 3). Protons with exchange rates too slow to be measured belong to the central core of the β-sheet. These residues exchange by a global-unfolding mechanism, which must show a free energy coincident with that obtained by thermal or chemical denaturation (Table 4). The remaining residues exchange by local-unfolding mechanisms, with apparent free energies lower than that obtained by CD denaturation equilibrium measurements.

An important aspect of the protein dynamics is the side-chain mobility. Side chains play key roles in many important processes, such as packing of hydrophobic residues at the interior of the protein, recognition and binding of other molecules, and enzymatic catalysis. Although we could not measure the $^3J_{\alpha\beta}$ coupling constants, some conclusions could be drawn from the low conformational flexibility of a number of side chains and their accessibility. The side chains of 48 residues are well-defined and show low conformational flexibility (χ_1 order parameter larger than 0.8). The majority of these residues are completely or partially buried, and they are located in regions of well-defined regular secondary structure, such as helices or β-strands. The side-chain conformation of aromatic residues, especially that of the Trp residues, is also well-defined. In the three tryptophan residues of thioredoxin *m*, the χ_2 angle is $\pm$90°, which appears to be its preferred conformation in most proteins (*56*).

Folding and Stability of Thioredoxin m. The criteria used to verify a two-state folding behavior include the coincidence of equilibrium denaturation transitions from different probes, the equivalence of the calorimetric and van't Hoff enthalpies, and the requirement that the free energy of unfolding and its dependence on equilibrium denaturation measurement be identical to that obtained from kinetic studies (*57*). We have

used several biophysical probes to follow the chemical denaturation of thioredoxin *m*. It is well-known that we can monitor by far-UV the secondary and/or tertiary structure depending on the observed wavelength, while by near-UV we are just observing the tertiary structure. In both cases, the obtained transition curves were superimposable (Figure 6B), what demonstrates that under equilibrium conditions the folding of thioredoxin is two-state.

Unfolding of thioredoxin *m* could not be followed by thermal denaturation, since no evidence of sigmoidal behavior was observed in the temperature range explored (25−85 °C). A high thermal midpoint has been observed in other thioredoxins, such as in *E. coli* thioredoxin, with a thermal midpoint of 88 °C (*58*), and in that from *B. acidocaldarius*, with 103 °C (*45*, *59*). We were able to determine the midpoint and the free energy of the transition by means of GdmCl denaturation (Table 4). The obtained values were higher than those measured for proteins of similar size but very similar to those measured in other thioredoxins. Thus, the midpoint in *E. coli* thioredoxin at neutral pH and the same temperature is 2.5 M (*60*), which is close to that obtained here for thioredoxin *m* in spinach (2.9 M). The high stability of the members of the thioredoxin family has been attributed to the tight packing of buried side chains and to the presence of an array of elements involved in hydrogen-bonded secondary structure. It will be interesting to determine whether other thioredoxins of superior plants share the same stability and the same fold. The knowledge of the solution structure described in this work will be the basis for further studies in our laboratory on the stability and folding of this thioredoxin, using mutants designed by protein engineering techniques.

In summary, we may conclude that thioredoxin *m* from spinach, the first thioredoxin of this class whose solution structure has been solved, displays a three-dimensional structure very close to that determined for other members of the family. This structure set the basis for future studies on the thermostability of thioredoxin and most importantly to understand the molecular interactions between this protein and NADP-dependent malate dehydrogenase and fructose-1,6-bisphosphatase or fragments from them, a first step toward a deep understanding of photosynthetic events in higher plants.

ACKNOWLEDGMENT

We gratefully acknowledge C. López, A. Gómez, and L. de la Vega for excellent technical assistance.

SUPPORTING INFORMATION AVAILABLE

Table S1, showing resonance assignments of thioredoxin *m*. This material is available free of charge via the Internet at http://pubs.acs.org.

REFERENCES

1. Eklund, H., Gleason, F. K., and Holmgren, A. (1991) *Proteins: Struct, Funct., Genet. 11*, 13−28.
2. Holmgren, A. (1989) *J. Biol. Chem. 264*, 13963−13966.
3. Holmgren, A., and Bjornstedt, M. (1995) *Methods Enzymol. 252*, 199−208.
4. Martin, J. L. (1995) *Structure 3*, 245−250.
5. Powis, G., and Montfort, W. R. (2001) *Annu. Rev. Biophys. Biomol. Struct 30*, 421−455.
6. Laurent, T. C., Moore, E. C., and Reichard, P. (1964) *J. Biol. Chem. 239*, 3436−3444.
7. Russel, M., Model, P., and Holmgren, A. (1990) *J. Bacteriol. 172*, 1923−1929.
8. Matthews, J. R., Wakasugi, N., Virelizier, J. L., Yodoi, J., and Hay, R. T. (1992) *Nucleic Acids Res. 20*, 3821−3830.
9. Russel, M., and Model, P. (1985) *Proc. Natl. Acad. Sci. U.S.A. 82*, 29−33.
10. Scheibe, R. (1991) *Plant Physiol. 96*, 1−3.
11. Buchanan, B. B. (1991) *Arch. Biochem. Biophys. 288*, 1−9.
12. Muller, E. G. D., and Buchanan, B. B. (1989) *J. Biol. Chem. 264*, 4008−4014.
13. Wolosiuk, R. A., Crawford, N. A., Yee, B. C., and Buchanan, B. (1979) *J. Biol. Chem. 254*, 1627−1632.
14. Knaff, D. B., and Hirasawa, M. (1991) *Biochim. Biophys. Acta 1056*, 93−125.
15. Rivera-Madrid, R., Mestres, D, Marinho, P., Jacquot, J.-P., Decottignies, P., Miginiac-Maslow, M., and Meyer, Y. (1995) *Proc. Natl. Acad. Sci. U.S.A. 92*, 5620−5624.
16. Lancelin, J. M, Stein, M., and Jacquot, J.-P. (1993) *J. Biochem. (Tokyo) 114*, 421−431.
17. Mittard., V., Morelle, N., Brutscher, B., Simorre, J.-P., Marion, D., Stein, M., Jacquot, J.-P., Lirsac, P.-N., and Lancelin, J.-M. (1995) *Eur. J. Biochem. 229*, 473−485.
18. Mittard, V., Blackedge, M. J., Stein, M., Jacquot, J.-P., Marion, D., and Lancelin, J.-M. (1997) *Eur. J. Biochem. 243*, 374−383.
19. Capitani, G., Markovic-Housley, Z., DelVal, G., Morris, M., Jansonius, J. N., and Schürmann, P. (2000) *J. Mol. Biol. 302*, 135−154.
20. Schurmann, P. (1995) *Methods Enzymol. 252*, 274−283.
21. Gill, S. C., and von Hippel, P. H. (1989) *Anal. Biochem. 182*, 319−326.
22. Marion, D., and Wüthrich, K. (1983) *Biochem. Biophys. Res. Commun. 11*, 967−975.
23. Rance, M., Sørensen, O. W., Bodenhausen, G., Wagner, G., Ernst, R. R., and Wüthrich, K. (1983) *Biochem. Biophys. Res. Commun. 117*, 479−485.
24. Bax, A., and Davis, D. G. (1985) *J. Magn. Reson. 65*, 355−360.
25. Jeener, J., Meier, B. H., Bachmann, P., and Ernst, R. R. (1979) *J. Chem. Phys. 71*, 4546−4553.
26. Piotto, M., Saudek, V., and Sklenar, V. (1993) *J. Biomol. NMR 2*, 661−665.
27. Wüthrich, K. (1986) *NMR of proteins and nucleic acids*, John Wiley and Sons, New York.
28. Wang, Y., Nip, A. M., and Wishart, D. S. (1997) *J. Biomol. NMR 10*, 373−382.
29. Wang, A., Robertson, A. D., and Bolen, D. W. (1995) *Biochemistry 34*, 15096−15104.
30. Nagayama, K., Kumar, A., Wüthrich, K., and Ernst, R. R. (1980) *J. Magn. Reson. 40*, 321−334.
31. Bai, Y., Milne, J. S., Mayne, L., and Englander, S. W. (1993) *Proteins: Struct., Funct., Genet. 17*, 75−86.
32. Hvidt, A., and Nielsen, S. O. (1966) *Adv. Protein Chem. 21*, 187−386.
33. Bartels, C., Xia, T., Billeter, M., Güntert, P., and Wüthrich, K. (1995) *J. Biomol. NMR 6*, 1−10.
34. Güntert, P., Braun, W., and Wüthrich, K. (1991) *J. Mol. Biol. 217*, 517−530.
35. Güntert, P., and Wüthrich, K. (1991) *J. Biomol. NMR 1*, 447−456.
36. Güntert, P, Berndt, K. D., and Wüthrich, K. (1993) *J. Biomol. NMR. 3*, 601−606.
37. Van Gusteren, W. F., and Berendsen, H. J. C. (1987) Groningen Molecular Simulation (GROMOS) Library Manual, Biomos, Groningen, The Netherlands.
38. Santoro, J., González, C., Bruix, M., Neira, J. L., Nieto, J. L., Herranz, J., and Rico, M. (1993) *J. Mol. Biol. 229*, 722−734.
39. Rico, M., Jiménez, M. A., González, C., De Filippis, V., and Fontana, A. (1994) *Biochemistry 33*, 14834−14847.

40. Padmanabhan, S., Jiménez, M. A., González, C., Sanz, J. M., Jiménez-Gallego, G., and Rico, M. (1997) *Biochemistry 36*, 6424−6436.
41. Koradi, R., Billeter, M., and Wüthrich, K. (1996) *J. Mol. Graphics 14*, 51−58.
42. Clarke, J., and Fersht, A. R. (1993) *Biochemistry 32*, 4322−4329.
43. Dyson, H. J., Holmgren, A., and Wright, P. E. (1989) *Biochemistry 28*, 7074−7087.
44. Katti, S. K., LeMaster, D. M., and Eklund, H. (1990) *J. Mol. Biol. 212*, 167−184.
45. Pedone, E. Bartolucci, S., Rossi, M., and Saviano, M. (1998) *J. Biomol. Struct. Dynam. 2*, 437−446.
46. Nicastro, G, Chiara, C., Pedone, E., Tatò, M., Rossi, M., and Bertolucci, S. (2000) *Eur. J. Biochem. 267*, 403−413.
47. Andersen, J. F., Sanders, D. A. R., Gasdaska, J. R., Weichsel, A., Powis, G., and Montfort, W. R. (1997) *Biochemistry 36*, 13979−13988.
48. Gronenborg, A. M., Clore, G. M., Louis, J. M., and Wingfield, P. T. (1999) *Protein Sci. 8*, 426−429.
49. Chaffotte, A. F., Li, J.-H., Georgescu, R. E., Goldberg, M. E., and Tasayco, M. L. (1997) *Biochemistry 36*, 16040−16048.
50. Kelly, S. M., and Price, N. C. (2000) *Curr. Protein Pept. Sci. 1*, 349−384.
51. Woody, R. W. (1995) *Methods Enzymol. 246*, 34−71.
52. Holmgren, A., and Bjornstedt, M. (1995) *Methods Enzymol. 252*, 199−208.
53. Dai, S., Schwendtmayer, C., Johansson, K., Ramaswamy, S., Schürmann, P., and Eklund, H. (2000) *Q. Rev. Biophys. 33*, 67−108.
54. Saarinen, M., Gleason, K., and Eklund, H. (1995) *Structure 3*, 1097−1108.
55. Qin, J., Clore, G. M., and Gronenborg, A. M. (1994) *Structure 2*, 503−522.
56. Ponder, J. W., and Richards, F. M. (1987) *J. Mol. Biol. 193*, 775−791.
57. Jackson, S. E., and Fersht, A. R. (1991) *Biochemistry 30*, 10428−10435.
58. Georgescu, R. E., Braswell, E. H., Zhu, D., and Tasayco, M. L. (1999) *Biochemistry 38*, 13355−13366.
59. Bartolucci, S., Guagliardi, A., Pedone, E., Depascale, D., Cannio, R., Camardella, L., Rossi, M., Nicastro, G., de Chiara, C., Facci, P., Mascetti, G., and Nicolini, C. (1997) *Biochem. J. 328*, 277−285.
60. Kelley, R. F., and Stellwagen, E. (1984) *Biochemistry 23*, 5095−5102.
61. Huyghues-Despointes, B. M. P., Scholtz, J. M., and Pace, C. N. (1999) *Nat. Struct. Biol. 6*, 910−912.
62. Englander, S. W., and Kallenbach, N. R. (1984) *Q. Rev. Biophys. 16*, 521−655.

BI011186X